

Evidence for Three Subpopulations of Globular Clusters in the Early-Type Post-Starburst Shell Galaxy AM 0139-655¹

Aparna Maybhate², Paul Goudfrooij², François Schweizer³, Thomas Puzia⁴, David Carter⁵

ABSTRACT

We present deep *Hubble Space Telescope* ACS images of the post-starburst shell galaxy AM 0139-655. We find evidence for the presence of three distinct globular cluster subpopulations associated with this galaxy: a centrally concentrated young population (~ 0.4 Gyr), an intermediate age population (~ 1 Gyr) and an old, metal-poor population similar to that seen around normal galaxies. The $g - I$ color distribution of the clusters is bimodal with peaks at 0.85 and 1.35. The redder peak at $g - I = 1.35$ is consistent with the predicted color for an old metal-poor population. The clusters associated with the peak at $g - I = 0.85$ are centrally concentrated and interpreted as a younger and more metal-rich population. We suggest that these clusters have an age of ~ 0.4 Gyr and solar metallicity based on a comparison with population synthesis models. The luminosity function of these “blue” clusters is well represented by a power law, $\phi(L)dL \propto L^{-1.8}dL$. Interestingly, the brightest shell associated with the galaxy harbors some of the youngest clusters observed. This seems to indicate that the same merger event was responsible for the formation of both the shells and the young clusters. The red part of the color distribution contains several very bright clusters, which are not expected for an old, metal-poor population. Furthermore, the luminosity function of the “red” GCs cannot be fit well by either a single gaussian or a single power law. A composite (gaussian + power law) fit to the luminosity function of the red clusters yields both a low rms and very

¹Based on observations with the NASA/ESA *Hubble Space Telescope*, obtained at the Space Telescope Science Institute, which is operated by the Association of Universities for Research in Astronomy, Inc., under NASA contract NAS5-26555

²Space Telescope Science Institute, Baltimore, MD 21218; maybhate@stsci.edu, goudfrooij@stsci.edu

³Carnegie Observatories, 813 Santa Barbara Street, Pasadena, CA 91101; schweizer@ociw.edu

⁴Herzberg Institute of Astrophysics, 5071 West Saanich Road, Victoria, BC V9E 2E7, Canada; puziat@nrc.ca

⁵Astrophysics Research Institute, Liverpool John Moores University, 12 Quays House, Egerton Wharf, Birkenhead, CH41 1 LD, United Kingdom; dxc@astro.livjm.ac.uk

plausible properties for an old population (with gaussian distribution) plus an intermediate-age population (with power-law distribution) of GCs. Hence, we suggest that the red clusters in AM 0139-655 consist of two distinct GC subpopulations, one being an old, metal-poor population as seen in normal galaxies and one having formed during a recent dissipative galaxy merger (likely the same event that formed the ~ 0.4 Gyr old clusters).

Subject headings: galaxies: elliptical and lenticular — galaxies: clusters: general — galaxies: individual(AM 0139-655) — galaxies: interactions — galaxies: star clusters

1. Introduction

Globular clusters (GCs) are very useful probes of the dynamical and chemical assembly histories of galaxies. Many globular cluster systems in “normal” giant elliptical galaxies show a bimodal color distribution, providing clear evidence for the presence of a “second event” during the formation of these systems (Ashman & Zepf 1998, and references therein). Spectroscopic studies have revealed that both the blue and red GC populations are typically old (≥ 8 Gyr, (Forbes et al. 2001; Cohen, Blakeslee, & Côte 2003; Puzia et al. 2005)) implying that the bimodality is mainly due to a difference in their metallicity. The merger scenario of Ashman & Zepf (1992) predicted the presence of this bimodal distribution. However, different theories were suggested by various authors to explain the nature of the second event. The merger model (Schweizer 1987; Ashman & Zepf 1992), predicts that the metal-rich clusters are formed during major mergers of gas-rich galaxies. The “multi-phase collapse” model (Forbes, Brodie, & Grillmair 1997) implies that they form during a secondary collapse phase of the galaxy, without invoking a merger event. The accretion scenario (Forte, Martinez, & Muzzio 1982; Côte, Marzke, & West 1998) proposes that every galaxy is born with a GC system that has a median color (metallicity) according to the color-magnitude relation of galaxies (e.g. Terlevich et al. 1999). The bimodality then arises due to the accretion of low-mass galaxies with metal-poor GCs by a larger galaxy with its metal-rich GCs.

Intermediate-age GCs have been found in several galaxies (Goudfrooij et al. 2001, 2007; Puzia et al. 2002; Kundu et al. 2005; Chandar et al. 2006). A few of these galaxies show features like shells or a disturbed morphology, indicating a recent merger event. Shells are sharply defined, arc-like features, mostly found around elliptical galaxies (Malin & Carter 1983), though a few (Arp 215, Arp 227) have been found around disk galaxies (Arp 1966). Two classes of models have been proposed to account for the shells. The internal models

(Fabian et al. 1980; Williams & Christiansen 1985) suggest that shell stars form because of star formation within a giant shell of shocked interstellar gas. On the other hand, the interaction models suggest an external origin for the shell structure and interpret it as arising due to a merger. When an elliptical galaxy accretes a small companion galaxy, some vestiges of the event survive for a Gyr or longer after the merger in the form of ripples and shells (Schweizer 1980; Quinn 1984). The morphology and alignment of the resulting shell system depends on the form of the potential of the primary galaxy, the orbital parameters of the collision and the nature of the companion (Hernquist & Quinn 1988, 1989; Dupraz & Combes 1986). Typical dynamical ages of shells are $0.5 - 2 \times 10^9$ years (Nulsen 1989; Hernquist & Quinn 1987). These shells, made up of stars, have been frequently observed around ellipticals. Malin & Carter (1983) find 17% and Schweizer & Ford (1985) find 44% of field ellipticals to be surrounded by shells. The presence of shells thus seems to be a common outcome of interactions of galaxies.

To test the merger scenario for GC formation, it is important to study galaxies that show obvious signs of a merger event in the form of shells, ripples, and some signature of having hosted a strong burst of star formation. One way of attempting this is to study E+A galaxies featuring shells. E+A galaxies were originally defined by the combination of an early-type galaxy morphology and the presence of a so-called “post-starburst” spectrum containing strong Balmer absorption lines (indicative of A-type stars) without strong [O II] or H α emission lines (Dressler & Gunn 1983)¹. The existence of strong Balmer absorption lines indicates that these galaxies have experienced star formation around $\sim 0.3 - 2$ Gyr ago while the absence of emission lines indicates that star formation must have ceased shortly thereafter. A large fraction (75%) of nearby E+A galaxies are located in the field (Zabludoff et al. 1996). Several of these show tidal features indicative of galaxy-galaxy interactions and mergers as the probable mechanism responsible for their formation.

Long-slit spectroscopy of E+A galaxies (Norton et al. 2001) revealed that the young stellar populations are typically more centrally concentrated than the old population, but are not always confined to the inner 1 kpc. Schiminovich et al. (1994) discovered atomic hydrogen associated with the shells of NGC 5128. Subsequently, CO molecules were found in two shells surrounding this elliptical providing evidence that the molecular gas in mergers may not only fall into the nucleus but can also be spread out to large galactocentric radii (Charmandaris et al. 2000). Carter et al. (1988) found evidence for recent nuclear star formation in 20 out of 100 shell galaxies in the Malin & Carter (1983) catalog, suggesting

¹ Subsequent studies revealed the presence of a disk component in many such galaxies, and many papers now use the term k+a, where the k stands for the spectral type of an old stellar population (e.g., Franx 1993).

that the process of shell formation may involve some accretion or merger of gas-rich material which would account for the nuclear star formation.

Numerical simulations of the sinking of a gas-rich satellite disk galaxy into a large elliptical galaxy by Kojima & Noguchi (1997) show that the stellar particles from the disk stars of the satellite start making a clear shell structure after the first collision with the elliptical in case of a radial or a retrograde merger. This shell system lasts for ~ 1 Gyr or more. They also find an abrupt reduction in the star formation rate around the time of first passage of the satellite through the center of the elliptical due to the sudden decrease in gas density caused by the gravitational scattering by the elliptical potential.

The study of GCs in such galaxies should yield important information regarding the nature of the E+A phenomenon. If numerous intermediate-age GCs with ages consistent with those of the post-starburst population in the nucleus were to be found, we could be fairly confident that the A stars were formed in a relatively vigorous and distinct star formation event, likely associated with a dissipative galaxy merger. Conversely, an absence of such GCs would indicate that no strong star formation was associated with the event that caused star formation to end ~ 0.5 to 2 Gyr ago. The latter would be consistent with a scenario where gas is removed from the galaxy, e.g. by ram pressure stripping. This paper focuses on a study of the globular cluster system of the early-type shell galaxy AM 0139-655.

2. AM 0139-655

AM 0139-655 (PGC 6240) is a giant early-type galaxy with bright shells that are irregularly distributed around the main body (Malin & Carter 1983). The nuclear spectrum of AM 0139-655 shows evidence for a post-starburst (E+A) spectrum with very strong Balmer absorption lines (suggesting the presence of a substantial fraction of A-type stars) but no significant [O II] emission (Carter et al. 1988). AM 0139-655 has a large H δ equivalent width (13.6 ± 1.0 Å) and an active nucleus. Since AM 0139-655 shows both shell structure (indicative of a merger) and a post-starburst spectrum (signaling a burst of star formation and hence possible globular cluster formation in the recent past), it is a good candidate to explore whether any relations exist between its globular cluster system, its morphology and the merger event that gave rise to the shells. In this paper, we present a detailed photometric study of the GCs of AM 0139-655. The general properties of AM 0139-655 are listed in Table 1.

3. Observations and Data Reduction

AM 0139-655 was observed with *HST* on July 16 and 17, 2004, as part of General Observer program 10227, using the Wide Field Channel (WFC) of ACS. It was observed for a total of 6 orbits in the continuous viewing zone (CVZ) of HST with total integration times of 21440 s in the F475W and 7300 s in the F814W filter. The observations consisted of several long exposures at different dither positions as well as a few short ones to prevent saturation of the galaxy center. The data were processed with the ACS on-the-fly pipeline which included dark and bias subtraction and flat fielding. Each flat-fielded image was carefully checked for satellite trails and saturated pixels in the central region of the galaxy. These pixels were flagged and masked out. The individual images in each band were co-added using the PyRAF task MULTIDRIZZLE (Koekemoer et al. 2002). This procedure removed all the cosmic rays and corrected for geometric distortion. The combination of the short and long exposure images enabled us to get good resulting multidrizzled images with unsaturated centers. The final combined F475W image is shown in Fig. 1.

4. Photometry

The search for sources was performed on an image made from the summed F475W+F814W image in the following manner. The F475W and the F814W images from multidrizzle were added together. To improve the detection and the accuracy of the photometry, especially for the faint sources embedded within the bright galaxy background, the underlying galaxy light was first modeled. Extensive experimentation showed that the application of a circular median filter gave the best results. Object detection was done by using the DAOIND routine in the DAOPHOT package (Stetson 1987) on an image obtained by dividing the combined image by the square root of the median filtered image (thus providing uniform shot noise characteristics over the whole frame). The advantage in using the $g+I$ image rather than the individual images for source detection is the greater depth reached by the combined image. Also, the photometric zero-point of $g+I$ is significantly less dependent on the color of the source than the individual g or I images, which helps during the completeness correction (see Goudfrooij et al. 2007 for a detailed discussion). The detection threshold was set at 4σ above the background. Typical half-light radii of globular clusters are in the range 1–20 pc (Kundu & Whitmore 2001; van den Bergh & Mackey 2004; Jordán et al. 2005). At the distance of AM 0139-655, the scale is 25 pc per ACS/WFC pixel. Thus, we expect the globular clusters to be nearly unresolved point sources on the image.

Smooth, median-filtered model images were created in each of the two bands from the corresponding multidrizzle combined images in a manner similar to the one described above.

The model was subtracted from the corresponding original images to get a residual image in which the galaxy light has been removed to a great extent and the compact objects are clearly visible. To confirm that the subtraction procedure did not alter the error statistics of the photometry, we compared the magnitudes obtained from the subtracted and the original images for a few bright sources in the frame. The differences between the two methods were well below the photometric errors. Aperture photometry was carried out on these residual images through an aperture of 3 pixel radius ($0''.15$). In order to discard obvious spurious detections (e.g. edges of the image), objects with magnitude errors greater than 0.4 mag were rejected at this point. Aperture corrections from 3 pixel ($0''.15$) to 10 pixel ($0''.5$) radius were determined using a few bright point sources in each band. The corrections from $0''.5$ to infinity were taken from Sirianni et al. (2005). The total aperture corrections were 0.470 ± 0.009 and 0.517 ± 0.010 in F475W and F814W respectively. The transformation from the instrumental magnitudes (STMAG) to SDSS g - and Cousins I -band was done using the SYNPHOT package in STSDAS. Synthetic spectra of stellar types ranging from B0V to K3III from the Bruzual & Charlot (1993) library were convolved with the SDSS g and the Cousins I filter to obtain magnitudes relative to Vega, and with the F475W and the F814W filters to yield magnitudes in the STMAG system. Fitting polynomials to get the relation between the two systems resulted in the following transformations:

$$\begin{aligned}
 g &= F475W + (0.4530 \pm 0.0006) \\
 &\quad + (0.039 \pm 0.001)(F475W - F814W) \\
 &\quad + (0.0010 \pm 0.0003)(F475W - F814W)^2 \\
 &\quad - (0.0040 \pm 0.0003)(F475W - F814W)^3 \\
 I &= F814W - (1.258 \pm 0.002) \\
 &\quad + (0.015 \pm 0.002)(F475W - F814W) \\
 &\quad - (0.002 \pm 0.003)(F475W - F814W)^2 \\
 &\quad - (0.001 \pm 0.001)(F475W - F814W)^3
 \end{aligned} \tag{1}$$

4.1. Globular Cluster Candidate Selection

The photometry lists with the magnitudes in g and I obtained in the preceding section also included foreground stars and extended objects, in addition to cluster candidates. To remove these contaminating sources we applied two selection criteria based on the FWHM and the compactness of each source. We obtained the direct FWHM of each of the sources

in the photometry list in each band using the task IMEXAM within IRAF² in batch mode. Since the FWHM of bright stars in our frame is ~ 2.0 pixels and we expect all the cluster candidates to be nearly unresolved point sources, we discarded all sources that did not satisfy the criterion $1.5 \leq \text{FWHM} \leq 3.0$ pixels. We also added a compactness criterion wherein only sources that had the difference in the magnitudes between aperture radii of 2 pixels and 5 pixels lie between 0.2 mag and 0.6 mag were retained. This ensured (to a great extent) that the contamination from background galaxies was minimized. To study the radial extent and distribution of the GC candidates so obtained, they were binned into annuli 400 pixels wide, starting from the center of the galaxy out to the corners of the ACS frame. An effective area was calculated for each annulus namely the total area of the pixels that lie within the annulus which had a non-zero value of intensity. This ensured that the masked-out regions like the chip gap were not considered while computing the area since these areas were also excluded during cluster finding. We plot the logarithm of the number of sources per kpc^2 as a function of the projected distance from the center of the galaxy and find that it reaches an asymptotic value at a projected radius of about 40 kpc (see Fig. 2). Given the large distance of the galaxy and hence, the small angular size of AM 0139-655, it was possible to use the outer parts of the image to estimate the contamination due to compact background sources.

From the Burstein & Heiles (1982) model, we find the Milky-Way foreground extinction $A_V = 0.00$. The resulting g versus $g-I$ color-magnitude diagram for the candidate globular clusters is shown in Fig. 3. The rectangle delineates the sources that meet our criteria for globular cluster candidates. Using the GALEV simple stellar population (SSP) models (Anders & Fritze-v. Alvensleben 2003), we determine the color range of $0 \leq g-I \leq 2.0$ to include all clusters over the range of ages from 10^7 to 10^{10} years and metallicity z values from 0.0004 to 0.05 (where $z = 0.02$ represents solar metallicity). All sources with colors redder than 2.0 are expected to be late-type foreground stars or red background galaxies and are rejected in the subsequent analysis. The final list, thus obtained, contains a total of 217 globular cluster candidates. Typical photometric errors in g were 0.01, 0.03, 0.15 and >0.2 mag for magnitude intervals 22-24 mag, 24-26 mag, 26-28.75 mag and fainter than 28.75 mag respectively. The brightest fifty GC candidates are listed in Table 2.

²IRAF is distributed by the National Optical Astronomy Observatories, which are operated by the Association of Universities for Research in Astronomy, Inc., under cooperative agreement with the National Science Foundation.

4.2. Completeness Corrections

Completeness tests were performed on the combined $g+I$ image, i.e., the one used for detection of cluster candidates. Artificial objects were added in batches of 100 for five background levels and several magnitude intervals. The background levels were computed from the $g+I$ image in the following manner. The counts in the outermost parts of the image, free from any galaxy light contamination were taken as Background level #1. The counts in the innermost region of the galaxy where clusters are detected were taken as Background level #5. This difference between the faintest and the brightest background levels was then divided into five equal intervals in log space to get the five mean background levels. The radial intensity profile of the artificial input globular clusters was determined by fitting PSFs to the cluster candidates in the original image. The image was divided by the square root of a median-filtered version of itself and source detection was performed on the resultant image, with the same procedure as used for the initial source finding. Further, the ranges of the FWHM, compactness and maximum permissible error in the derived magnitudes were also selected in exactly the same manner as that for the actual source photometry. The resultant completeness curves are shown in Fig. 4.

5. $g-I$ Color Bimodality

To analyze the color distribution of globular clusters in AM 0139-655, we start by computing the non-parametric Epanechnikov-kernel probability density function \mathcal{P}_{obj} of all objects inside the analysis radius of 40 kpc (Silverman 1986). Given the photometric completeness of our data \mathcal{P}_{obj} is the closest approximation to the real color distribution of globular clusters. The width of the adaptive kernel linearly depends on the statistical color uncertainty of every individual object, so that the initial noise statistics of the color measurements is translated into the final probability density estimate. To account for uncertainties due to the limited sample size, we bootstrapped this process 100 times and derive 90% confidence limits of the resulting probability density function.

With the same technique we also computed the probability density function of the background field \mathcal{P}_{bkg} derived from the detections. We then scaled the background density estimate to the object function \mathcal{P}_{obj} by area. We note that the error associated with the scaling of the function is included in our bootstrap routine and propagated to the uncertainty of the final density estimate. We finally derive the color distribution of globular cluster candidates by statistical subtraction:

$$\mathcal{P}_{\text{GCC}} = \mathcal{P}_{\text{obj}} - A\mathcal{P}_{\text{bkg}} \quad (2)$$

where A is the ratio of areas encompassed by the object versus background regions. Figure 5 shows the background corrected function. The final color distribution appears clearly extended and, taking the 90% error margins into account, bimodal with peaks at $g-I = 0.85$ and $g-I = 1.35$. A rather extensive red wing to the red peak is present, which will be discussed in Sect. 7. KMM tests (McLachlan & Basford 1988; Ashman et al. 1994) were also run on the background subtracted $g-I$ color distribution. The KMM test for two components resulted in peak values consistent with those found using the Epanechnikov kernel. The test for three components resulted in a third peak with $g-I = 1.45$ but without any clusters assigned to it.

Although we do not know the effects of possible internal extinction on individual GCs, the fact that the blue peak of the GC color distribution found in AM 0139-655 at $g-I = 1.35$ is consistent with $V-I = 0.95$ (for 14 Gyr old, metal-poor clusters from SSP models) which agrees with the blue peak of GCs in the Milky-Way indicates that on average the internal visual extinction is very small. At the same time, this also supports our assumption that the Milky-Way foreground extinction is near zero, as predicted by the Burstein & Heiles (1982) model.

5.1. Spatial Distribution of the Blue and Red Subpopulations

As shown in the preceding section, the color distribution of the clusters has a bimodal form with peaks near $g-I = 0.85$ and 1.35 . The spatial distributions of the two subpopulations were derived by dividing the clusters into two subpopulations based on their colors. Clusters which lie in the range $0 \leq g-I \leq 0.95$ were designated as the blue population and those within $1.15 \leq g-I \leq 2.0$ were designated as the red population. The region $0.95 < g-I < 1.15$ was avoided to minimize mixing of the two populations. This yielded 84 blue clusters, 114 red clusters and 19 clusters that lie in the region of mixing.

Figure 2 shows the radial distribution of the blue and red samples. The bins were chosen in such a way that there were at least five clusters in each bin in the region within 40 kpc. It is clear from the figure that the blue clusters are more concentrated towards the center and their surface density falls as we go away from the center. On the other hand, the surface density of the red clusters is somewhat low in the center and may peak between 5-10 kpc from the center of the galaxy. The surface density distribution of the 19 GCs that lie in the intermediate color range is also shown in Fig. 2. This distribution appears to peak at the center. Adding all these clusters to the blue clusters would not change the trend for the blue clusters while adding them to the red clusters would tend to somewhat dilute the effect in the central regions.

We used the SSP models described in Anders & Fritze-v. Alvensleben (2003) to estimate the ages of the two populations. These models include continuum and line emission and take into account the important contribution of gaseous emission to broad-band fluxes and their strong metallicity dependence during the very early evolutionary stages of star clusters. The top panel of Fig. 6 shows the dependence of $g-I$ color on the age of the cluster. From the figure, we see that the red peak in the color distribution at $g-I = 1.35$ can be explained by clusters of age 14 Gyr and metallicity $Z = 0.0004$ which agrees very well with the colors expected for the old, metal-poor globular cluster population that forms the blue peak in normal ellipticals or spirals. The blue peak of the color distribution at $g-I = 0.85$ can be explained by a younger population of clusters of solar metallicity with an age ~ 0.4 Gyr. Note that this age estimate is fairly independent of the metallicity: See Fig. 6. This is consistent with the E+A nature of AM 0139-655. We assume solar metallicity for these clusters since several spectroscopic studies of luminous intermediate-age globular clusters in a number of merger remnants have shown that they have near-solar metallicities (NGC 7252 (Schweizer & Seitzer 1998); NGC 3921 (Schweizer et al. 2004); NGC 1316 (Goudfrooij et al. 2001) and NGC 5128 (Peng et al. 2004)). *HST* imaging studies of the same merger remnants show that these young clusters are more concentrated towards the galaxy center than the old metal-poor clusters (Miller et al. 1997; Schweizer et al. 1996; Goudfrooij et al. 2001; Peng et al. 2004), as predicted by Ashman & Zepf (1992) who modeled the formation of clusters in a dissipative galaxy merger.

Figure 7 shows the projected spatial distribution of the blue and the red clusters while Fig. 8 shows the $g-I$ color map obtained by dividing the g image by the I image. In Fig. 8, note the presence of a blue ring-like structure surrounding the center and the blue clusters present along the ring. Another interesting fact is that the brightest and the most distinct shell (lying between 14.8-16.7 kpc to the East of the galaxy center) harbors seven blue clusters (Fig. 9), all of which fall within the color range $0.70 \leq g-I \leq 0.91$, consistent with SSP model ages between 0.25-0.4 Gyr. Thus, it appears that all the clusters associated with this shell were formed during the latest burst of star formation. We suggest that the same event that formed the shell structure also gave rise to the young globular cluster population.

6. Luminosity Function of AM 0139-655

To derive the luminosity functions (LFs) of the clusters, we proceeded in the following manner. A completeness correction was applied to each cluster depending on its magnitude and background level. This was determined from the curves shown in Fig. 4 using bilinear interpolation. The clusters were then divided into two groups depending on their distance

from the galaxy center. The clusters within a projected distance of 40 kpc from the center of the galaxy were considered as actual GC candidates and the ones farther were considered as contaminants (foreground stars and compact background galaxies). The LFs of the GC candidates were then corrected for background contamination using the smoothed and scaled LFs of these objects. The LFs obtained after completeness and background contamination correction and the uncorrected LFs in the I -band are shown in Fig. 10.

Given the distance modulus of 35.3 for AM 0139-655, the globular cluster turn-over magnitude for old, metal-poor GCs is expected at $I = 27.2$ (for $M_I = -8.1$) (Harris 1996). As seen from the figure, the data does not quite reach the peak of the turnover. We analyze the luminosity functions of the blue and red clusters separately.

6.1. Luminosity Function of the Blue Clusters

As mentioned above in Section 5.1, all clusters with colors in the range $0.0 \leq g-I \leq 0.95$ are considered as blue clusters. Figure 10 (middle panel) shows the luminosity function of these blue clusters. A power-law fit to the LF of the blue clusters yields $\phi(L)dL \propto L^{-\alpha} dL$ with $\alpha = -1.8 \pm 0.1$, consistent with the results of previous LF studies of young clusters in mergers and merger remnants which find power-law indices in the range $-2.1 < \alpha < -1.7$ (Whitmore & Schweizer 1995; Meurer et al. 1995; Whitmore et al. 1999; Whitmore 2003).

6.2. Luminosity Function of the Red Clusters

Clusters within the color range $1.15 \leq g-I \leq 2.0$ were classified as red clusters and their luminosity functions derived (Fig. 10, bottom panel). Attempts to fit their luminosity function by either a single gaussian or a single power law yielded large residuals. Upon close examination of the color-magnitude diagram, we found a significant number of very luminous red clusters. If the red clusters were attributed solely to an old, metal-poor population, with a mass function similar to that in our Galaxy, the brightest clusters would not be expected to be brighter than $M_g = -10.0$ ($g = 25.0$), yet we find an excess of clusters as bright as $g = 23.5$. In addition, the color distribution of the red clusters shows a broad tail towards red colors (Fig. 5) which suggests the presence of more than one sub-population.

6.2.1. Modeling the Composite Luminosity Function

Spectroscopic studies of intermediate-age clusters in NGC 1316 (Goudfrooij et al. 2001) and NGC 5128 (Peng et al. 2004) have shown that they have near-solar metallicities. Simulations of the color-magnitude diagrams of evolving clusters by Whitmore et al. (1997) show that solar metallicity clusters in the age range of 1-2 Gyr are the most difficult to identify since they have nearly the same colors as the old, metal-poor GC subpopulation. However, they are significantly (2-2.5 mag) brighter than the old ones for a given mass. Whitmore et al. (1997) also find that solar metallicity clusters older than ~ 2 Gyr will be redder than the old, metal-poor cluster population. Using the SSP models shown in Fig. 6, we see that the range of colors corresponding to the red cluster distribution in AM 0139-655 can indeed be explained by a metal-poor population about 14 Gyr old, but also by a metal-rich younger population about 1-1.5 Gyr old. To test whether our observed distribution may indeed be the result of two distinct populations of the same color but different ages and metallicities, we model the observed luminosity function as a combination of two populations; one old, metal-poor population which is consistent with a gaussian magnitude distribution and the other an intermediate-age population of solar metallicity, which can be described by a power law (e.g. Goudfrooij et al. 2004).

To constrain the possible relative contributions of the two populations, we consider the specific frequency of GCs,

$$S_N = N_{GC} 10^{0.4(M_V + 15)} \quad (3)$$

i.e., the number of star clusters per galaxy luminosity normalized to an absolute V magnitude of -15 (Harris & van den Bergh 1981). To estimate the contribution of the old, metal-poor cluster population to the mixed luminosity function, we need to first consider the possible S_N values of the progenitors and their V magnitude. Assuming AM 0139-655 was formed by a merger of two galaxies, the progenitor galaxies could have been two spirals or one elliptical and one spiral. Since there is no a priori obvious way of determining the nature of the progenitors, we consider various scenarios.

The specific frequency is known to increase systematically along the Hubble sequence, from 0.5 ± 0.2 for Sc spirals to 2.6 ± 0.5 for ellipticals outside of clusters (Harris 1991). Hence, we consider four values of S_N (0.25, 0.5, 1.0 and 3.0) covering the range from spirals to ellipticals to describe the possible specific frequencies of the progenitors. We use the V magnitude of AM 0139-655 to estimate the combined V magnitude of the progenitors. This will be a rough estimate and will tend to overestimate the luminosity since star formation during the merger would brighten the merger remnant. However, the V magnitude of AM 0139-655 is not listed in the literature. Hence, we first calculate the total g and I magnitudes of AM 0139-655 from our images using ellipse fits and calculate $g-I$ from these magnitudes.

We get $g = 13.64$; $I = 12.34$ and hence, $g - I = 1.30$.

Using this, we find the luminosity-weighted age of 1 Gyr for a solar metallicity population at this $g - I$ from Fig. 6. A 1 Gyr solar metallicity population has $V - I = 0.89$ and hence $V = 13.23$ according to the GALEV models. We then compute the fading in the V band from this age to an age of 14 Gyr from the lower panel of Fig. 6. We use luminosity-weighted age at solar metallicity as we are attempting to separate the intermediate-age clusters (which should have about solar metallicity) from the old, metal-poor GC population. Though a SSP is not a very good approximation to a galaxy, it is sufficient for our purpose since we are interested in getting a rough estimate of the fading of the galaxy. Using the faded value of $V = 15.84$ ($M_V = -19.45$), in the equation for S_N , we calculate the number of old globular clusters expected for the four values given above. The estimated gaussians for the old, metal-poor population were calculated using $M_I = -8.1$ and $\sigma = 1.2$ (Harris 1996; Barmby, Huchra, & Brodie 2001) for each S_N . Fig. 11 shows the observed luminosity function of the red clusters and the estimated gaussians for the four values of S_N . Subtracting the contributions to the gaussians in each case and examining the residuals, we find that the residuals in each case can be fit by power laws with power-law indices α between -1.6 and -1.85 consistent with values found for intermediate-age cluster populations. The rms values of the difference between the power law fits and the histograms in the right panel of Fig. 11 are 4.08, 2.88, 3.28 and 3.02 for $S_N = 3.0, 1.0, 0.5$ and 0.25 respectively. The above analysis suggests that the red cluster population in AM 0139-655 is in fact a combination of two populations of different ages. To conclude, we have identified three populations of GCs in AM 0139-655: one blue, metal-rich population of young clusters and a red population that can be split into two populations, one old (14 Gyr) metal-poor and one of intermediate age (1-1.5 Gyr) and solar metallicity. Since the two populations contributing to the red peak had similar colors, the KMM test could not identify them as separate populations. The estimates of ages, metallicities and the number of clusters (corrected for background contamination and completeness) belonging to the three sub-populations are given in Table 3 for the various possible scenarios. However, spectroscopic observations of the brightest candidates from the three populations will be necessary to derive exact metallicities and verify our tentative interpretation.

6.3. Masses of the Clusters

It is illustrative to estimate the masses of the bright clusters formed during the merger and compare them to the masses of the most massive clusters in our Galaxy (ω Cen with a mass $5 \times 10^6 M_\odot$) and M31 (Mayall II, G1), with a mass $(1.4 - 1.7) \times 10^7 M_\odot$ (Meylan et al.

2001).

Fig. 12 shows curves of constant mass superimposed on the color-magnitude diagram. To derive these masses, a grid was constructed for the observed magnitude and color range. These magnitudes were then faded to an age of 14 Gyr. Masses were assigned to each cluster by assuming the value of M/L_V to be 4.1 (at 14 Gyr), as found by Meylan et al. (1995). We find that several clusters in AM 0139-655 will have masses greater than that of the most massive cluster in our galaxy and comparable to the most massive cluster G1 in M31 when they age to 14 Gyr without subsequent mass loss due to stellar evolution since this mass loss is small beyond 1 Gyr (Anders & Fritze-v. Alvensleben 2003). The clusters will lose stars during their dynamical evolution. Their stellar-dynamical mass loss, however, cannot be evaluated with any confidence without orbital information.

The masses derived in this way have two caveats. First, the mass-to-light ratio is assumed to be equal to that of ω Cen. Various studies (Meylan et al. 1991) find a wide range (1.2 to 5.2) of mass-to-light ratios for GCs. According to Bruzual & Charlot (2003) models computed using the Chabrier (2003) IMF and lower and upper mass cut-offs $m_L = 0.1M_\odot$ and $m_U = 100M_\odot$, M/L_V of a 14 Gyr solar metallicity population is 4.3 while that of a $1/50 Z_\odot$ population of the same age is 2.0. Hence, a mass-to-light ratio of 4.1 is a good approximation for solar metallicity clusters. In the absence of any spectroscopic data on these clusters, these values can be taken as rough estimates. Secondly, the effects of internal reddening (though expected to be small from Sect. 5), have not been taken into account. This is not expected to change the mass ranges much since dereddening would tend to shift the points to brighter magnitudes and bluer colors (upward and to the left in Fig. 12), which is nearly parallel to the curves of equal mass.

7. Nature of the Progenitors

In a recent study of GC systems around six shell ellipticals, Sikkema et al. (2006) typically find bimodal distributions similar to those of normal ellipticals. They find some indications of the presence of a younger intermediate-age globular cluster population in two of their galaxies, but the number of these intermediate-age clusters is small as compared to the old clusters. However, in the case of AM 0139-655, we find that the cluster system is dominated by the young and the intermediate-age clusters with a relatively small contribution from the old, metal-poor clusters. In order to constrain the number of old, metal-rich clusters that might have been inherited from the progenitors, we note that there is some evidence for a small peak which is consistent with a redder, metal-rich sub-population (at $g-I = 1.8$) as expected for a sub-solar metallicity from the SSP models. The small number of GCs in this

minor peak suggests the absence of a significant bulge in either precursor. Additionally, for the four values of S_N considered for modeling the LF of the precursors, the rms values point out that at least one of the progenitors was not an elliptical, but had small S_N values ≤ 1 , which is consistent with Hubble types of Sb or later (Chandar et al. 2004; Goudfrooij et al. 2003) which have small bulges. Both the above findings seem to suggest that the galaxies involved in the merger that formed AM 0139-655 did not have a large bulge generally seen in early-type galaxies but were most likely late-type spirals with small bulges. A merger involving late-type gas-rich spirals could have formed one population of new GCs about 1 Gyr ago in a starburst at first pericenter and another one 0.4 Gyr ago at final merging (Mihos & Hernquist 1996).

From the fact that we see evidence for a young and intermediate-age component of clusters in AM 0139-655, we can safely assume that at least one of the galaxies involved in the recent interaction must have been rich in gas since there were two episodes of star formation within the time periods for shell survival. This is also supported by the fact that AM 0139-655 itself has strong Balmer absorption lines, which suggests that at least one of the progenitors must have been gas-rich and hence could not have been an early-type with a large bulge.

8. Summary and Conclusions

Deep ACS images of the post-starburst shell galaxy AM 0139-655 have been analyzed. We find a total of 217 GC candidates associated with this galaxy. The $g-I$ color distribution of the clusters shows two distinct peaks, one at $g-I = 0.85$ and the other at $g-I = 1.35$. We compare the colors with SSP models and find that the red peak coincides with the color expected of the old, metal-poor population. The blue peak corresponds to a young population (0.4 Gyr) assuming solar metallicity. The luminosity function of the blue clusters can be fit by a power law of index $\alpha \sim -1.8 \pm 0.1$, as is expected for young clusters. The red part of the distribution shows a long tail and the presence of several luminous clusters. We show that the luminosity function of the red clusters can be modeled as a combination of two subpopulations: An old population with a gaussian distribution and an intermediate-age population with a power law distribution. Thus, three subpopulations of globular clusters are clearly distinguishable in AM 0139-655. The number of clusters in the old, metal-rich subpopulation that is commonly associated with “normal” early-type galaxies is very small relative to the three aforementioned subpopulations. The combination of this dearth of old, metal-rich clusters and the fact that the LF of the old population is best fit by a small value of S_N supports the notion that any bulge in the progenitor galaxies must have been small.

The ages of the two younger GC subpopulations are comparable to typical lifetimes of shell structures formed during simulations of galaxy mergers, and the brightest shell actually seems to host several young GCs. This strongly suggests that both the shells and the young and intermediate-age GCs were formed during a dissipative merger. It thus seems fairly likely that the E+A signatures of this galaxy are due to this recent merger. These findings lend credence to the “merger scenario” for the formation of metal-rich GCs and their galaxy hosts.

We would like to thank the referee, Uta Fritze for useful comments. We would like to thank Rupali Chandar and Diane Karakla for useful discussions. Support for this work was provided by NASA through HST grant number GO-10227 from the Space Telescope Science Institute, which is operated by the Association of Universities for Research in Astronomy, Inc., under NASA contract NAS5-26555.

Facilities: HST (ACS).

REFERENCES

Anders, P., & Fritze-v. Alvensleben, U. 2003, A&A, 401, 1063

Arp, H. 1966, ApJS, 123, 1

Ashman, K.M., & Zepf, S.E. 1992, ApJ, 384, 50

Ashman, K.M., Bird, C.M., & Zepf, S.E. 1994, AJ, 108, 2348

Ashman, K.M., & Zepf, S.E. 1998, In *Globular Cluster Systems*, (Cambridge Univ. Press, Cambridge)

Barmby, P., Huchra, J.P., & Brodie, J. P. 2001, AJ, 121, 1482

Bruzual, G. A., & Charlot, S. 1993, ApJ, 405, 538

Bruzual, G. A., & Charlot, S. 2003, MNRAS, 344, 1000

Burstein, D., & Heiles, C. 1982, AJ, 87, 1165

Carter, D., Prieur, J.L., Wilkinson, A., Sparks, W.B., & Malin, D.F. 1988, MNRAS, 235, 813

Chabrier, G. 2003, PASP, 115, 763

Chandar, R., Puzia, T.H., Sarajedini, A., & Goudfrooij, P. 2006, ApJ, 646, 107

Chandar, R., Whitmore, B., & Lee, M.G. 2004, ApJ, 611, 220

Charmandaris, V., Combes, F., & van der Hulst, J.M. 2000, A&A, 35, L1

Cohen, J.G., Blakeslee, J.P., & Côte, P. 2003, ApJ, 592, 866

Côte, P., Marzke, R.O., & West, M.J. 1998, ApJ, 501, 554

Dressler, A., & Gunn, J.E. 1983, ApJ, 270, 7

Dupraz, C., & Combes, F. 1986, A&A, 166, 53

Fabian, A.C., Nulsen, P.E.J., & Stewart, G.C. 1980, Nature, 287, 613

Forbes, D.A., Beasley, M.A., Brodie, J.P., & Kissler-Patig, M. 2001, ApJ, 563, L143

Forbes, D. A., Brodie, J.P., & Grillmair, C.J. 1997, AJ, 113, 1652

Forte, J.C., Martinez, R.E., & Muzzio, J.C. 1982, AJ, 87, 1465

Franx, M. 1993, PASP, 105, 1058

Goudfrooij, P., Mack, J., Kissler-Patig, M., Meylan, G., & Minniti, D. 2001, MNRAS, 322, 643

Goudfrooij, P., Strader, J., Brenneman, L., Kissler-Patig, M., Minniti, D., & Huizinga, E.J. 2003, MNRAS, 343, 665

Goudfrooij, P., Gilmore, D., Whitmore, B.C., Schweizer, F. 2004, ApJ, 613, L121

Goudfrooij, P., Schweizer, F., Gilmore, D., & Whitmore, B.C. 2007, *astro-ph/0702467*

Harris, W.E., & van den Bergh, S. 1981, AJ, 86, 1627

Harris, W.E. 1991, ARA&A, 29, 543

Harris, W.E. 1996, AJ, 112, 1487

Hernquist, L., & Quinn, P.J. 1987, ApJ, 312, 1

Hernquist, L., & Quinn, P.J. 1988, ApJ, 331, 682

Hernquist, L., & Quinn, P.J. 1989, ApJ, 342, 1

Jordán, A., Côte, P., Blakeslee, J. P.. et al. 2005, ApJ, 634, 1002

Koekemoer, A.M., Fruchter, A.S., Hook, R.N., & Hack, W. 2002, in *The 2002 HST Calibration Workshop: Hubble after the Installation of the ACS and the NICMOS Cooling System*, ed. S. Arribas, A. Koekemoer, & B. Whitmore (Baltimore: Space Telescope Science Institute), p.337

Kojima, M., & Noguchi, M. 1997, ApJ, 481, 132

Kundu, A., & Whitmore, B. C. 2001, AJ, 121, 2950

Kundu, A., Zepf, S.E., Hempel, M., et al. 2005, ApJ, 634, L41

Malin, D.F., & Carter, D. 1983, ApJ, 274, 534

McLachlan, G. J., & Basford, K. E. 1988, In: *Mixture Models: Inference and Application to Clustering* (New York: Dekker)

Meurer, G.R., Heckman, T.M., Leitherer, C., Kinney, A., Robert, C., & Garnett, D.R. 1995, AJ, 110, 2665

Meylan, G., Dubath, P., & Mayor, A. 1991, ASPC, 13, 158

Meylan, G., Mayor, M., Duquennoy, A., & Dubath, P. 1995, A&A, 303, 761

Meylan, G., Sarajedini, A., Jablonka, P., Djorgovski, S.G., Bridges, T., & Rich, R.M. 2001, AJ, 122, 830

Mihos, J.C., & Hernquist, L. 1996, ApJ, 464, 641

Miller, B.W., Whitmore, B.C., Schweizer, F., & Fall, S.M. 1997, AJ. 114, 2381

Norton, S.A., Gebhardt, K., Zabludoff, A.I., & Zaritsky, D. 2001, ApJ, 557, 150

Nulsen, P.E.J. 1989, ApJ, 346, 690

Peng, E.W., Ford, H.C., & Freeman, K.C. 2004, ApJ, 602, 705

Prieur, J.-L. 1990, In: *Dynamics and Interactions of Galaxies*, ed. R. Wielen, Springer-Verlag Berlin, p. 72

Puzia, T.H., Zepf, S.E., Kissler-Patig, M., Hilker, M., Minniti, D., & Goudfrooij, P. 2002, A&A, 391, 453

Puzia, T.H., Kissler-Patig, M., Thomas, D., Maraston, C., Saglia, R.P., Bender, R., Goudfrooij, P., & Hempel, M. 2005, A&A, 439, 997

Quinn, P. 1984, ApJ, 279, 596

Salpeter, E.E. 1955, ApJ, 121, 161

Schiminovich, D., van Gorkom, J.H., van der Hulst, J.M., & Kasow, S. 1994, ApJ, 423, 101

Schweizer, F. 1980, ApJ, 237, 303

Schweizer, F., & Ford, W.K. 1985, in *New Aspects of Galaxy Photometry*, ed. J.-L. Nieto, New York:Springer-Verlag, p. 145

Schweizer, F. 1987, In: *Nearly Normal Galaxies* ed. by S.M. Faber (Springer, New York) p.18

Schweizer, F., Miller, B.W., Whitmore, B.C., & Fall, S.M. 1996, AJ, 112, 1839

Schweizer, F., & Seitzer, P. 1998, AJ, 116, 2206

Schweizer, F., Seitzer, P., & Brodie, J.P. 2004, AJ, 128, 202

Sikkema, G., Peletier, R.F., Carter, D., Valentijn, E.A., & Balcells, M. 2006, A&A, 458, 53

Silverman, B.W. 1986, In: *Density Estimation for Statistics and Data Analysis*, Chap and Hall/CRC Press, Inc.

Sirianni, M., et al. 2005, PASP, 117,1409

Stetson, P.B. 1987, PASP, 113, 1420

Terlevich, A.I., Kuntschner, H., Bower, R.G., Caldwell, N., & Sharples, R.M. 1999, MNRAS, 310, 445

van den Bergh, S., & Mackey, A. D. 2004, MNRAS, 354, 713

Whitmore, B.C., & Schweizer, F. 1995, AJ, 109, 960

Whitmore, B.C., Miller, B.W., Schweizer, F., & Fall, S.M. 1997, AJ, 114, 1797

Whitmore, B.C., Zhang, Q., Leitherer, C., Fall, S.M., Schweizer, F., & Miller, B.W. 1999, AJ, 118, 1551

Whitmore, B.C. : The Formation of Star Clusters, In: *A Decade of HST Science* ed. by M.Livio et al. (Cambridge Univ. Press, Cambridge 2003) p.153

Williams, R.E., & Christiansen, W.A. 1985, ApJ, 291, 80

Zabludoff, A.I., Zaritsky, D., Lin, H., Tucker, D., Hashimoto, Y., Shectman, S.A., Oemler, A., & Kirshner, R.P. 1996, ApJ, 466, 104

Table 1. General properties of AM 0139-655.

Parameter	Value
RA*(J2000)	1h 41m 30.98s
Dec*(J2000)	$-65^{\circ} 36' 55.44''$
Hubble Type	S0
v_{hel}	$8216 \pm 15 \text{ km s}^{-1}$
v_{hel} (corr)	7936 km s^{-1}
velocity dispersion	$249 \pm 46 \text{ km s}^{-1}$
Distance**	105.8 Mpc
$m-M$	35.3
scale	$1'' = 512 \text{ pc}$ $1 \text{ ACS pixel} = 25 \text{ pc}$
M_B	-20.57
galactic latitude (b)	-50.7°
A_v^{***}	0.00

*From ACS images, this work.

**Using $H_0 = 75 \text{ km s}^{-1} \text{Mpc}^{-1}$

***Burstein & Heiles (1982)

Note. — All other parameters are taken from LEDA (<http://leda.univ-lyon1.fr/>)

Table 2. Positions and photometry of the 50 brightest globular cluster candidates

RA (2000)	Dec (2000)	<i>I</i> (mag)	<i>g</i> – <i>I</i> (mag)	<i>r</i> *(‘‘)	<i>r</i> ** (kpc)
1 41 30.55	-65 36 45.99	20.87 ± 0.01	1.17 ± 0.02	9.82	5.0
1 41 30.03	-65 35 54.43	20.94 ± 0.01	1.11 ± 0.02	61.29	31.4
1 41 31.13	-65 36 51.80	21.12 ± 0.01	0.97 ± 0.02	3.77	1.9
1 41 27.32	-65 37 41.27	21.18 ± 0.01	1.34 ± 0.02	51.10	26.1
1 41 31.79	-65 36 51.03	21.61 ± 0.01	0.86 ± 0.02	6.68	3.4
1 41 33.59	-65 36 20.00	21.68 ± 0.01	1.20 ± 0.02	38.96	19.9
1 41 31.42	-65 36 55.59	21.75 ± 0.03	1.62 ± 0.07	2.72	1.4
1 41 41.69	-65 37 15.45	21.95 ± 0.01	0.69 ± 0.02	69.30	35.5
1 41 28.43	-65 36 46.53	22.30 ± 0.01	1.83 ± 0.02	18.14	9.3
1 41 30.32	-65 36 53.15	22.31 ± 0.02	0.82 ± 0.02	4.69	2.4
1 41 24.96	-65 36 20.35	22.46 ± 0.01	0.80 ± 0.02	51.20	26.2
1 41 24.19	-65 37 29.70	22.67 ± 0.01	1.29 ± 0.02	54.23	27.7
1 41 21.20	-65 37 32.10	22.68 ± 0.01	1.85 ± 0.02	70.79	36.2
1 41 30.46	-65 36 57.50	22.93 ± 0.02	0.44 ± 0.03	3.82	1.9
1 41 29.46	-65 36 40.09	23.00 ± 0.02	0.80 ± 0.02	18.01	9.2
1 41 31.12	-65 36 52.59	23.24 ± 0.03	0.98 ± 0.04	2.98	1.5
1 41 31.78	-65 36 58.93	23.25 ± 0.02	0.81 ± 0.03	6.05	3.1
1 41 29.62	-65 37 3.23	23.33 ± 0.02	0.88 ± 0.02	11.44	5.8
1 41 31.33	-65 37 24.40	23.42 ± 0.02	1.60 ± 0.03	29.03	14.8
1 41 26.70	-65 36 25.75	23.48 ± 0.02	0.95 ± 0.03	39.80	20.4
1 41 24.35	-65 36 23.94	23.55 ± 0.02	0.97 ± 0.03	51.72	26.5
1 41 21.14	-65 37 18.86	23.57 ± 0.02	1.37 ± 0.03	65.24	33.4
1 41 26.62	-65 36 5.87	23.66 ± 0.02	1.07 ± 0.03	56.46	28.9
1 41 27.33	-65 36 38.57	23.67 ± 0.02	1.15 ± 0.03	28.21	14.4
1 41 35.83	-65 36 49.06	23.67 ± 0.02	0.77 ± 0.03	30.74	15.7
1 41 30.67	-65 36 58.31	23.68 ± 0.04	0.31 ± 0.05	3.45	1.7
1 41 30.16	-65 36 54.38	23.72 ± 0.03	0.96 ± 0.04	5.20	2.6
1 41 29.12	-65 37 30.60	23.81 ± 0.02	1.30 ± 0.03	36.99	18.9
1 41 30.15	-65 36 59.70	23.85 ± 0.02	1.40 ± 0.04	6.68	3.4
1 41 36.63	-65 36 58.83	23.95 ± 0.02	1.30 ± 0.03	35.15	18.0
1 41 36.02	-65 36 46.84	23.97 ± 0.02	0.83 ± 0.03	32.40	16.6

Table 2—Continued

RA (2000)	Dec (2000)	I (mag)	$g - I$ (mag)	$r^*(")$	r^{**} (kpc)
1 41 35.53	-65 36 49.60	24.02 ± 0.02	0.82 ± 0.03	28.78	14.7
1 41 26.32	-65 36 59.17	24.06 ± 0.02	1.37 ± 0.03	29.06	14.9
1 41 35.04	-65 36 47.56	24.10 ± 0.02	1.35 ± 0.03	26.35	13.5
1 41 21.85	-65 36 2.19	24.10 ± 0.02	1.23 ± 0.03	77.69	39.8
1 41 29.50	-65 36 52.78	24.12 ± 0.03	0.85 ± 0.03	9.51	4.8
1 41 22.49	-65 37 31.88	24.15 ± 0.02	1.97 ± 0.04	63.96	32.7
1 41 32.33	-65 36 49.64	24.16 ± 0.02	0.94 ± 0.03	10.18	5.2
1 41 29.73	-65 36 48.36	24.17 ± 0.03	1.39 ± 0.04	10.49	5.4
1 41 42.40	-65 37 29.54	24.26 ± 0.02	1.74 ± 0.04	78.53	40.2
1 41 31.52	-65 37 0.55	24.26 ± 0.03	0.93 ± 0.04	6.11	3.1
1 41 33.11	-65 37 37.96	24.35 ± 0.03	1.36 ± 0.04	44.52	22.8
1 41 24.02	-65 36 42.34	24.40 ± 0.03	1.35 ± 0.04	45.02	23.0
1 41 29.77	-65 37 9.49	24.42 ± 0.03	1.38 ± 0.04	15.90	8.1
1 41 29.56	-65 37 1.17	24.47 ± 0.03	0.85 ± 0.04	10.45	5.3
1 41 20.68	-65 36 45.31	24.50 ± 0.03	1.64 ± 0.04	64.55	33.0
1 41 28.81	-65 37 3.23	24.51 ± 0.03	0.73 ± 0.04	15.49	7.9
1 41 38.81	-65 37 12.53	24.56 ± 0.03	1.54 ± 0.04	51.41	26.3
1 41 34.14	-65 35 44.84	24.57 ± 0.03	1.20 ± 0.04	73.27	37.5
1 41 24.77	-65 36 31.55	24.57 ± 0.03	1.72 ± 0.05	45.29	23.2

*projected radius derived using the position of the center at RA = 1h 41m 30.98s and Dec = $-65^\circ 36' 55.44''$

**Using $H_0 = 75 \text{ km s}^{-1}\text{Mpc}^{-1}$

Table 3: Properties of the three sub-populations of GCs

	Age (Gyr)	Z	N
Old	14	0.0004	25 (for $S_N = 1.00$)
			12 (for $S_N = 0.50$)
			6 (for $S_N = 0.25$)
Intermediate	1––1.5	0.02	81 (for $S_N = 1.00$)
			93 (for $S_N = 0.50$)
			99 (for $S_N = 0.25$)
Young	0.4	0.02	50

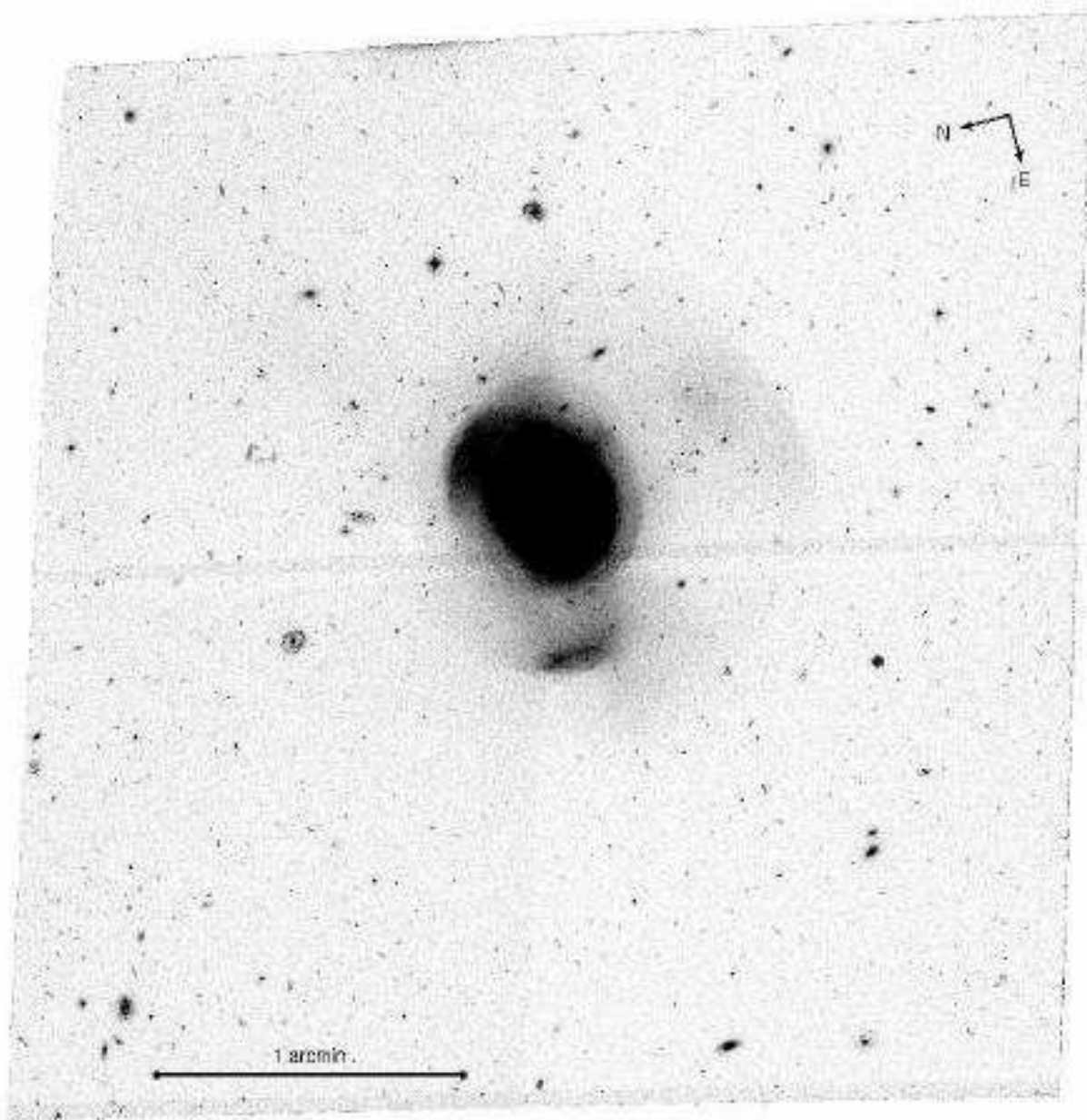


Fig. 1.— ACS image of AM 0139-655 in F475W

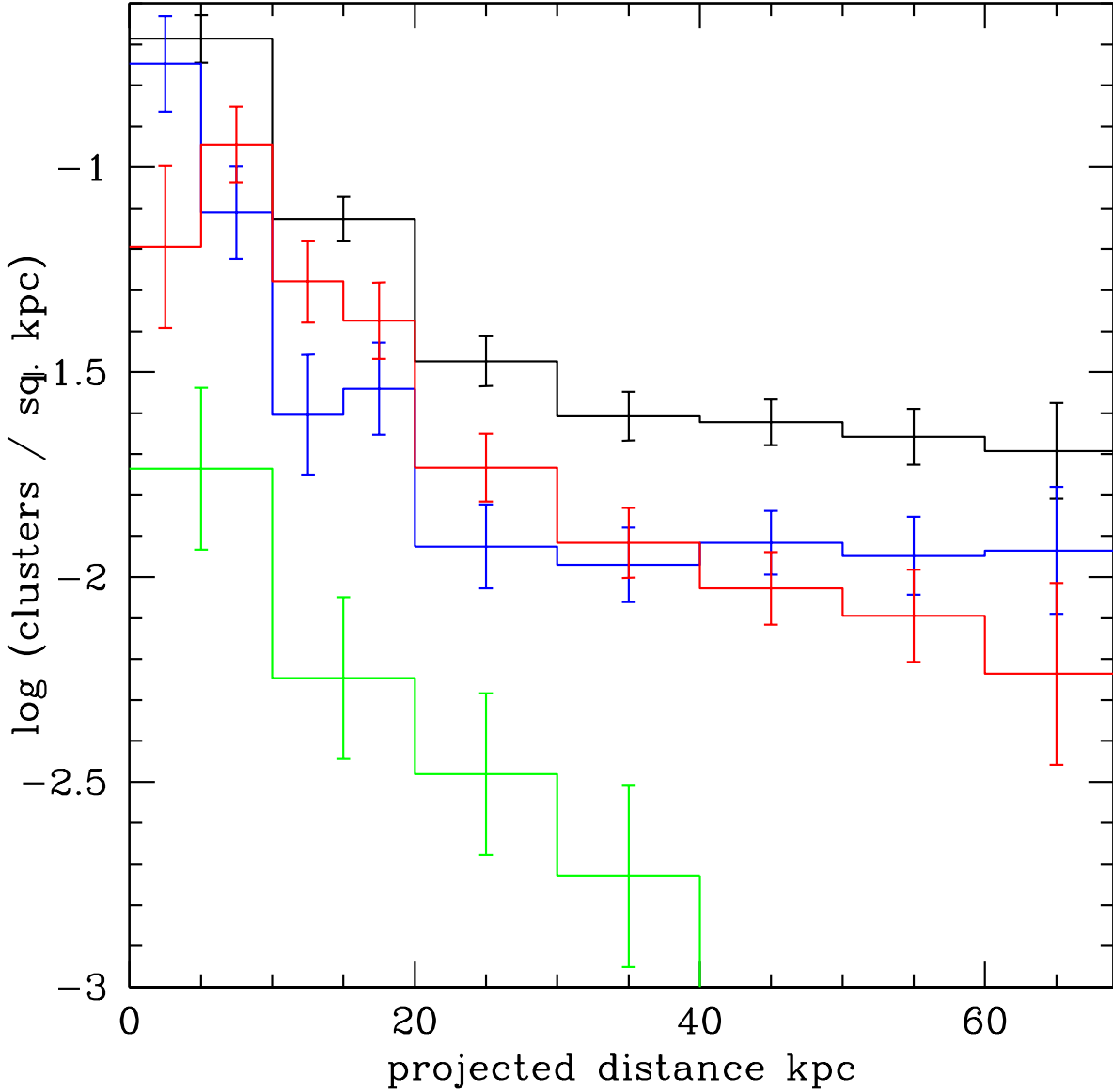


Fig. 2.— Surface density of the globular cluster candidates as a function of the distance from the galaxy center. The black solid line shows all the clusters, the blue line shows the distribution of the blue clusters and the red line shows the distribution of the red clusters. The surface density of clusters lying in the color range $0.95 < g-I < 1.15$ (between the blue and the red clusters) is shown by the green line. The bin width is 10 kpc except for the inner 20 kpc for the blue and the red clusters where it is 5 kpc. The blue clusters seem to be more centrally concentrated as compared to the red clusters.

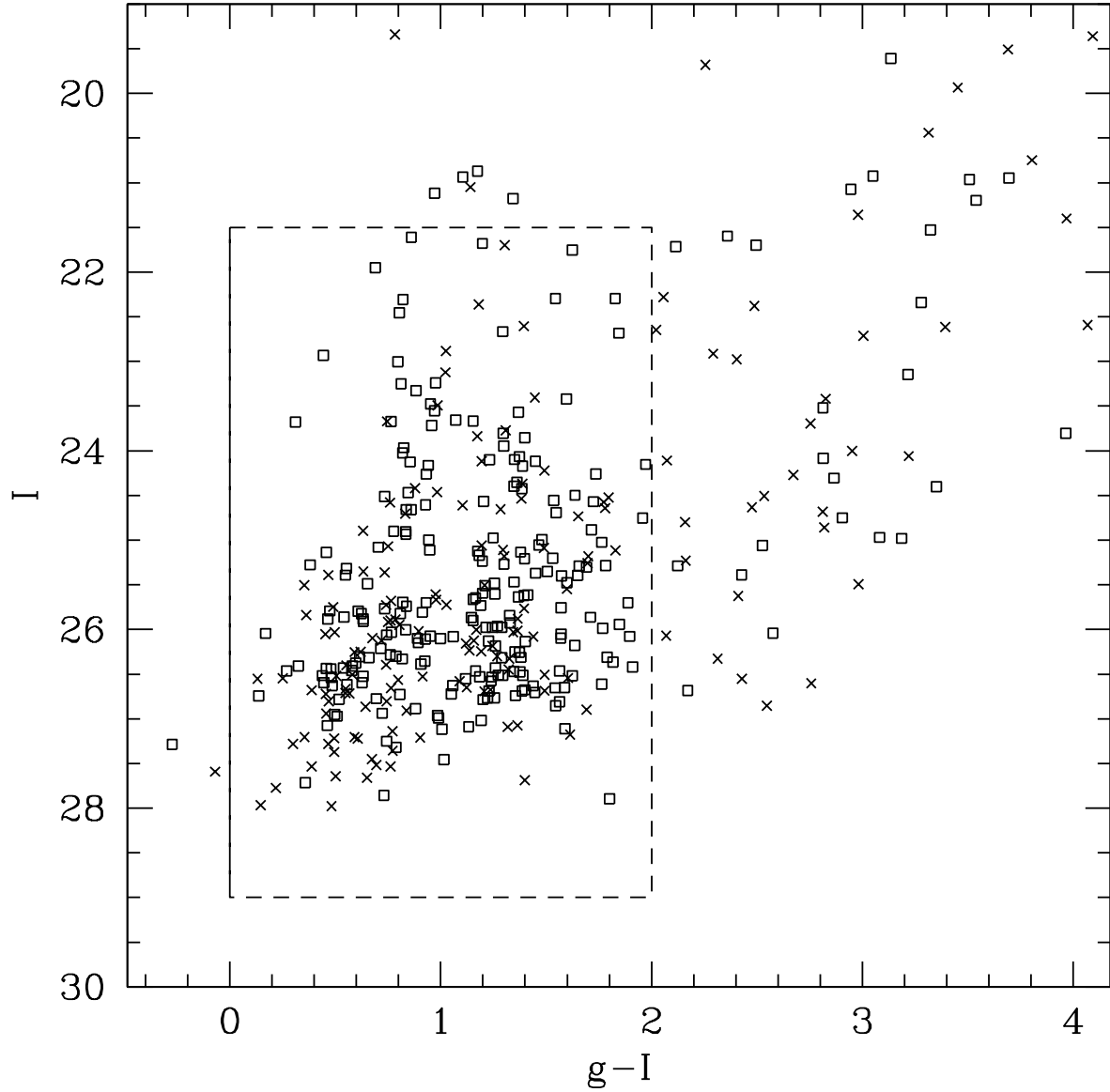


Fig. 3.— g versus $g-I$ color-magnitude diagram for AM 0139-655 globular cluster candidates. The open squares denote GC candidates present within the inner 40 kpc and the crosses denote those present beyond 40 kpc. The dotted lines delineates the region of GC selection.

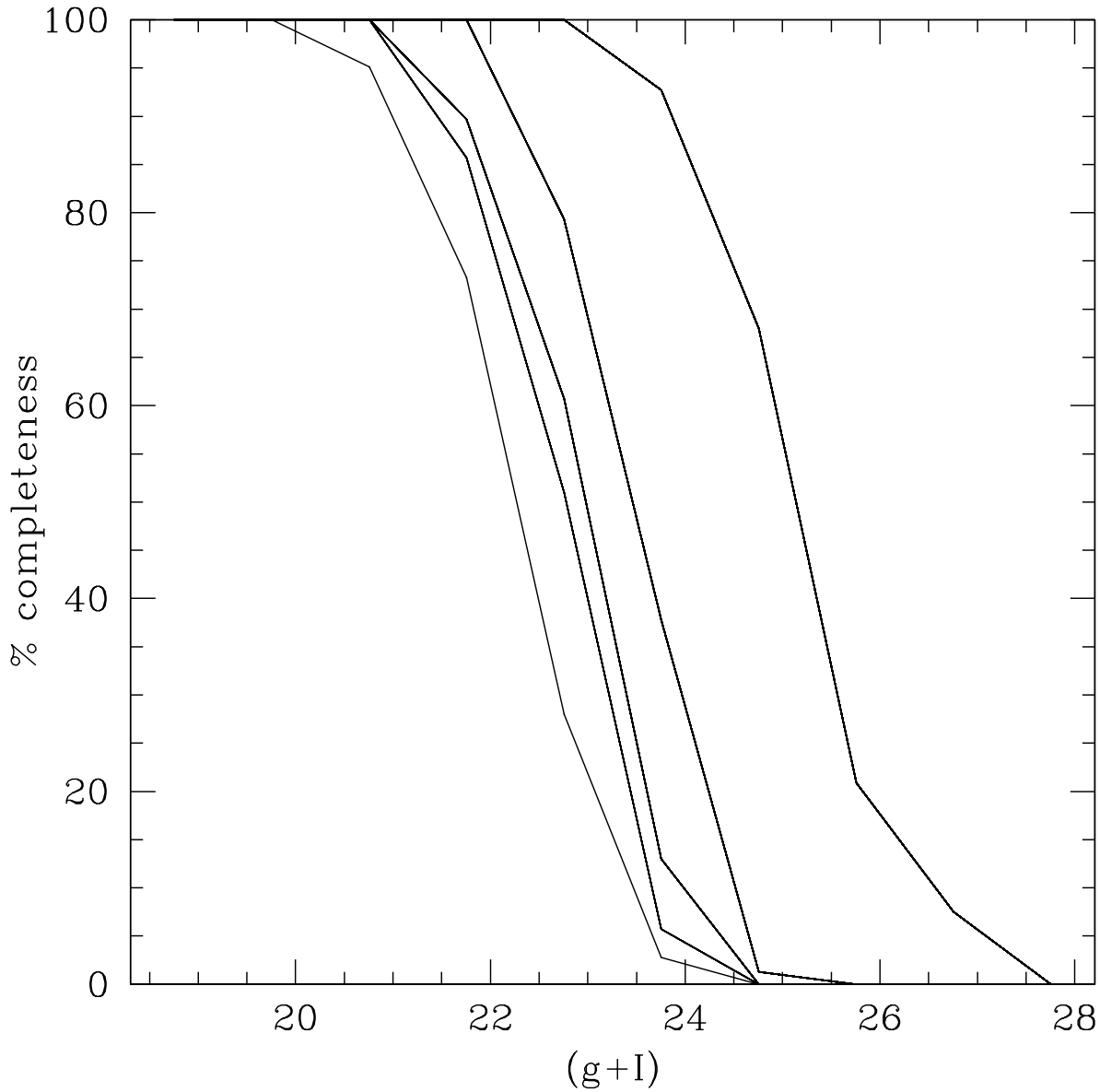


Fig. 4.— Completeness correction curves for the combined g and I band for five background levels. From left to right: 2000, 980, 480, 200, 120 e^- per pixel for an effective $g+I$ exposure time of 1822 s.

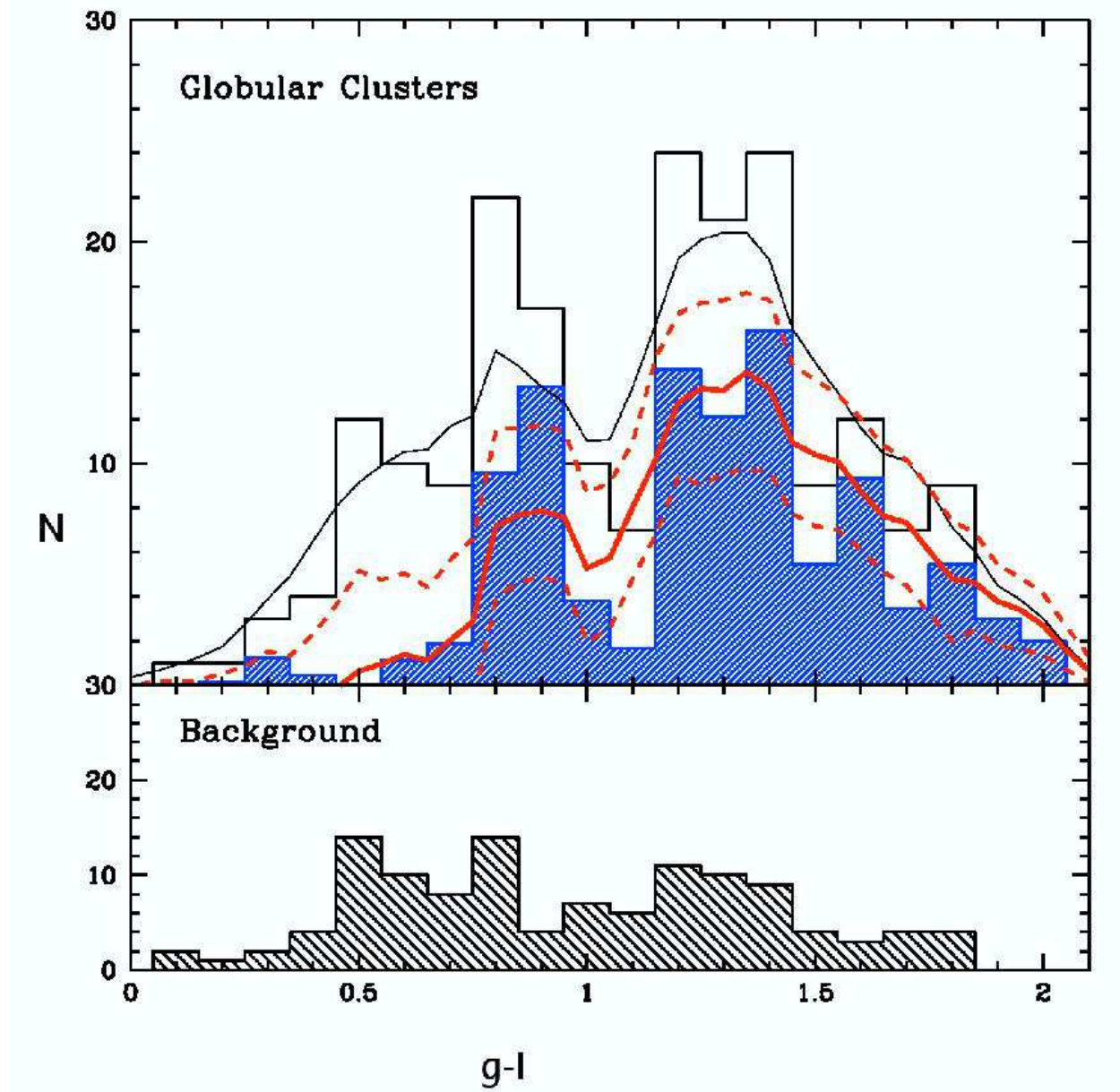


Fig. 5.— GC color distribution for AM 0139-655. The open histogram in the top panel represents the observed color distribution and the hatched histogram represents the distribution after subtraction of the background. The background distribution is shown in the lower panel. The solid red line is a non-parametric probability density estimate using an adaptive Epanechnikov kernel of the background corrected GC color distribution. The dashed red lines mark the bootstrapped 90% confidence limits. The solid black line represents the probability density estimate of the uncorrected distribution. Two peaks are clearly seen at $g-I = 0.85$ and $g-I = 1.35$. Note that the distribution of red clusters has a broad tail. There is a very faint signature of the redder, metal-rich peak that is seen in normal ellipticals at $g-I \approx 1.8$. This suggests that one or both of the progenitors had only a small bulge.

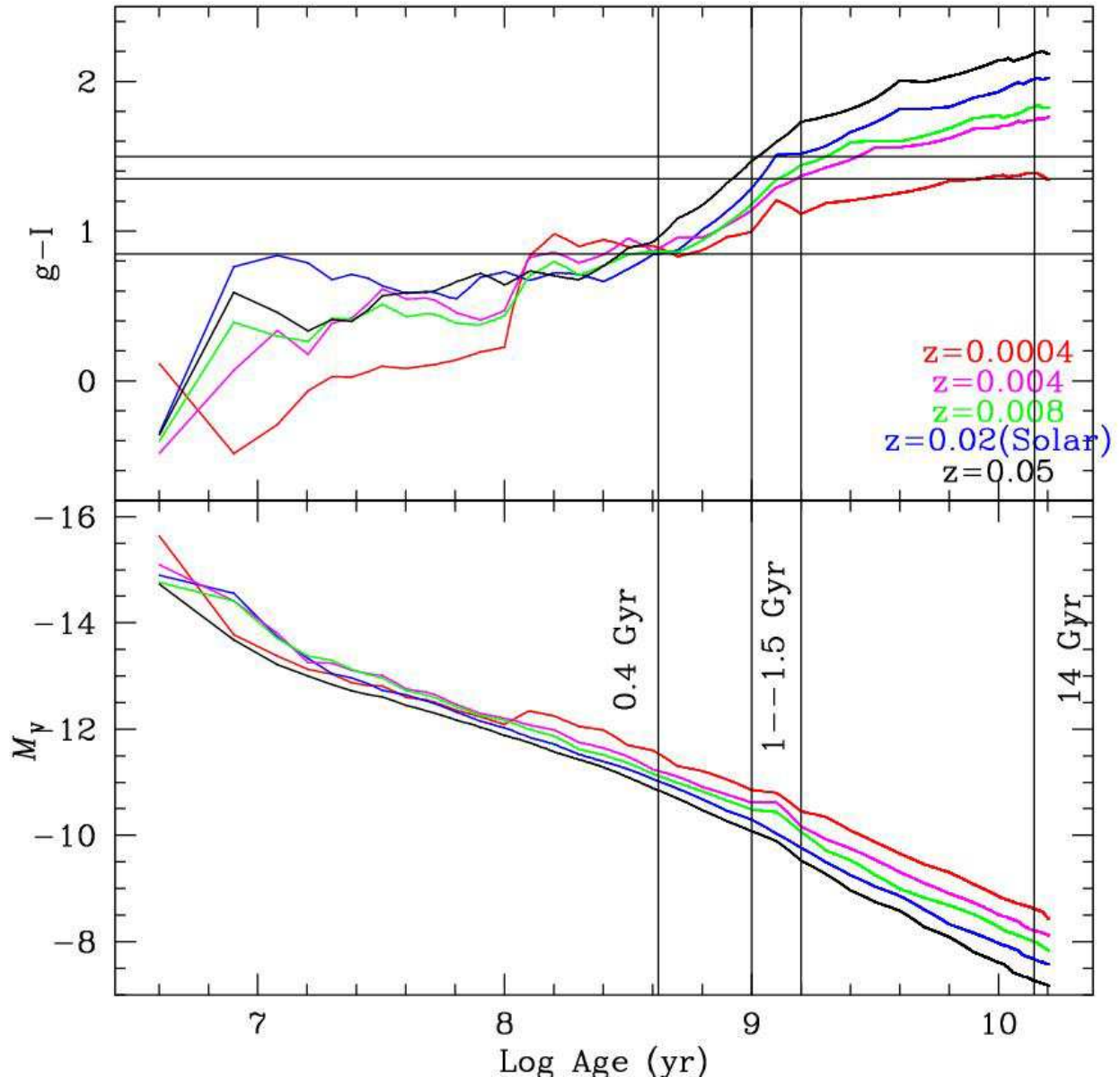


Fig. 6.— Time evolution of the $g - I$ color index (top panel) and absolute magnitude M_V per $1 \times 10^6 M_\odot$ of single-burst stellar population models using GALEV (Anders & Fritze-v. Alvensleben 2003). Model curves are plotted for a (Salpeter 1955) IMF and metallicities as indicated in the figure. Ages of the three stellar populations are indicated by 0.4 Gyr, 1-1.5 Gyr and 14 Gyr for the youngest, the intermediate and the old population respectively. The evolution of the V magnitude, predicted from the same models is shown in the bottom panel and is used to compute the fading of various clusters to an age of 14 Gyr.

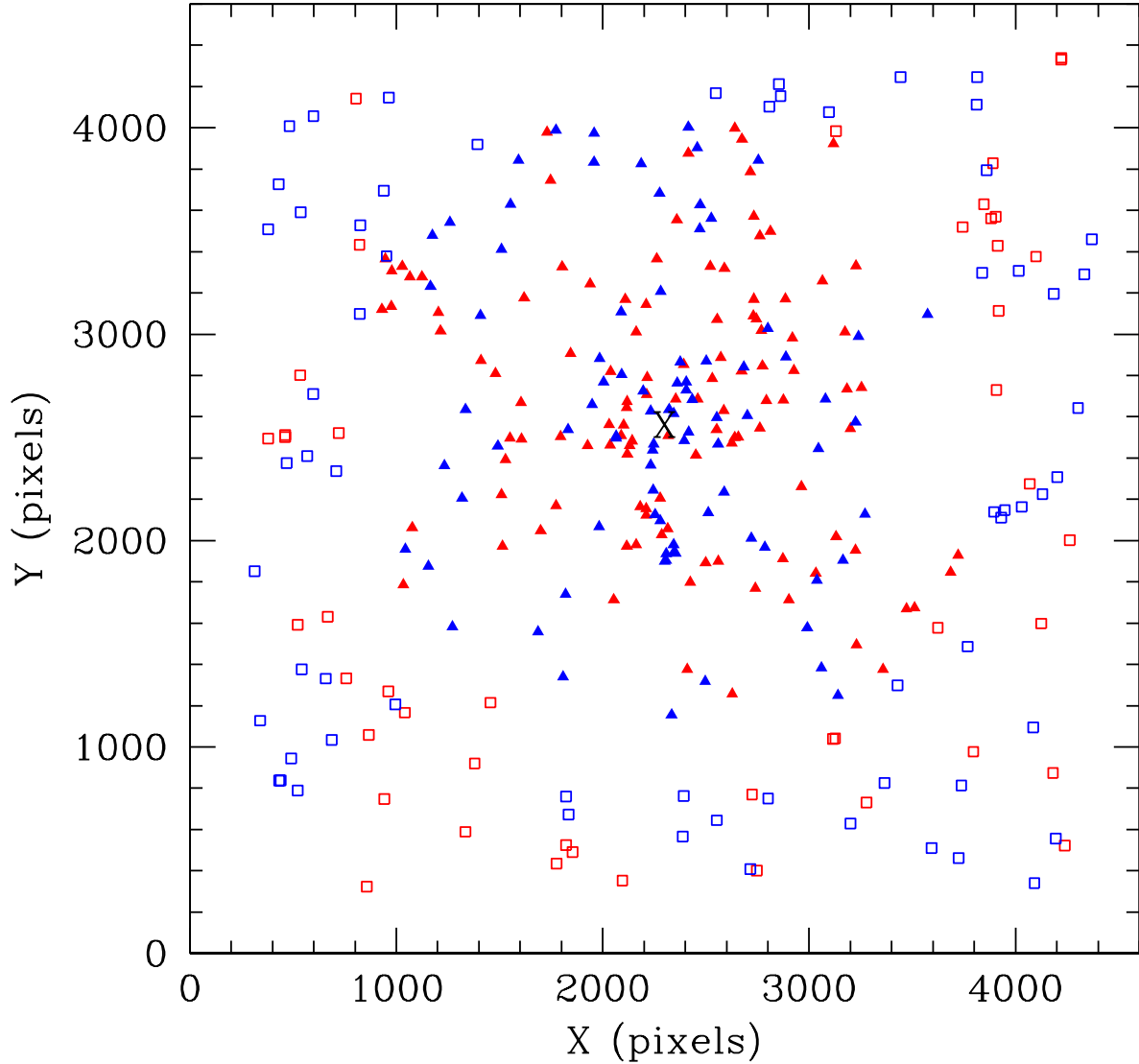


Fig. 7.— The projected spatial distribution of the clusters on the ACS image. “X” denotes the galaxy center. The red and blue filled triangles stand for the red and the blue clusters, respectively. The open red and blue squares are the red and blue objects in the background region where the surface number density of clusters is approximately constant.

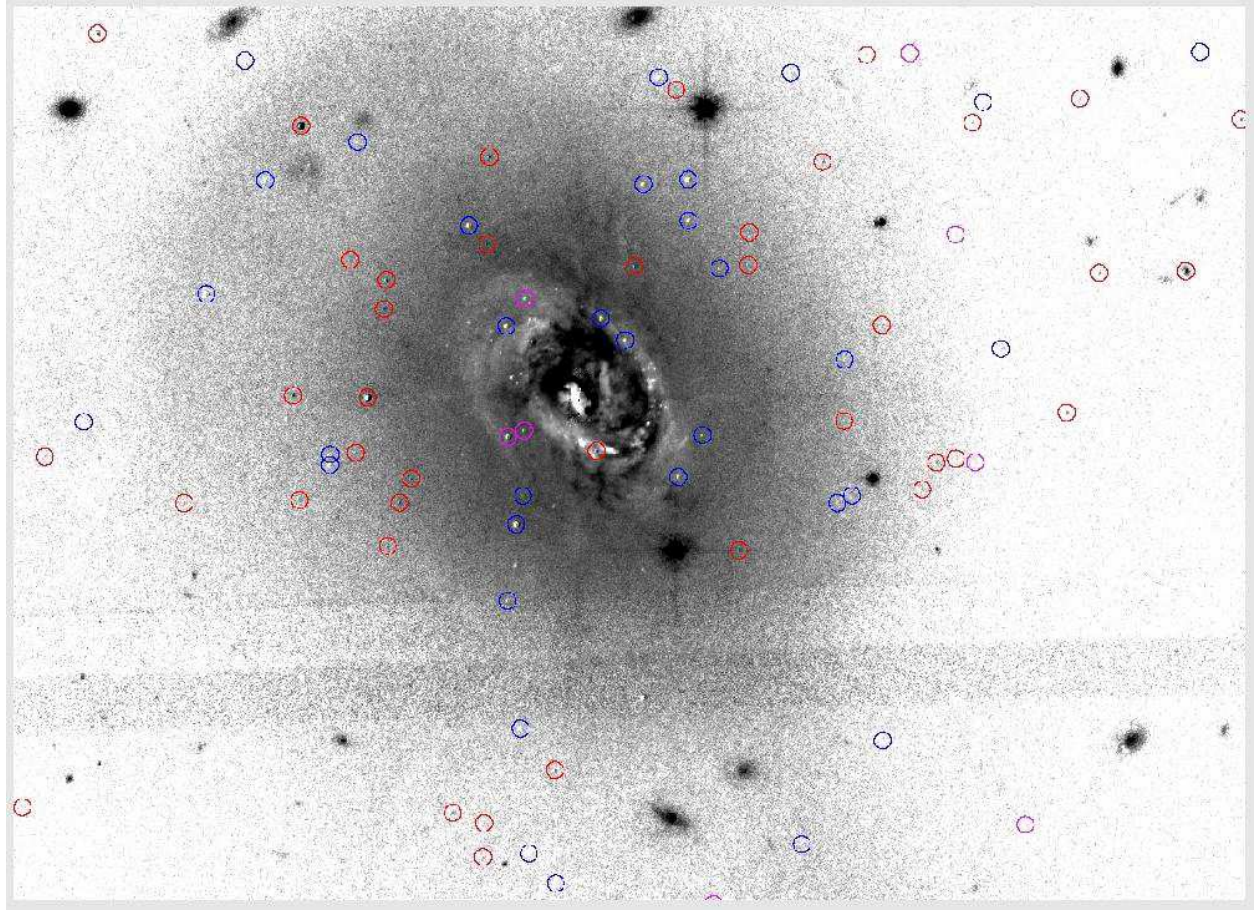


Fig. 8.— $g-I$ image of the inner region of AM 0139-655 showing the locations of the globular cluster candidates in the inner region. The dark regions denote redder colors, and the light regions denote bluer colors. The blue, red and magenta circles represent blue clusters, red clusters and clusters with $g-I$ between 0.95 and 1.15. The bright region in the center is the nucleus of AM 0139-655. Note the presence of several clusters along the blue ring surrounding the center.

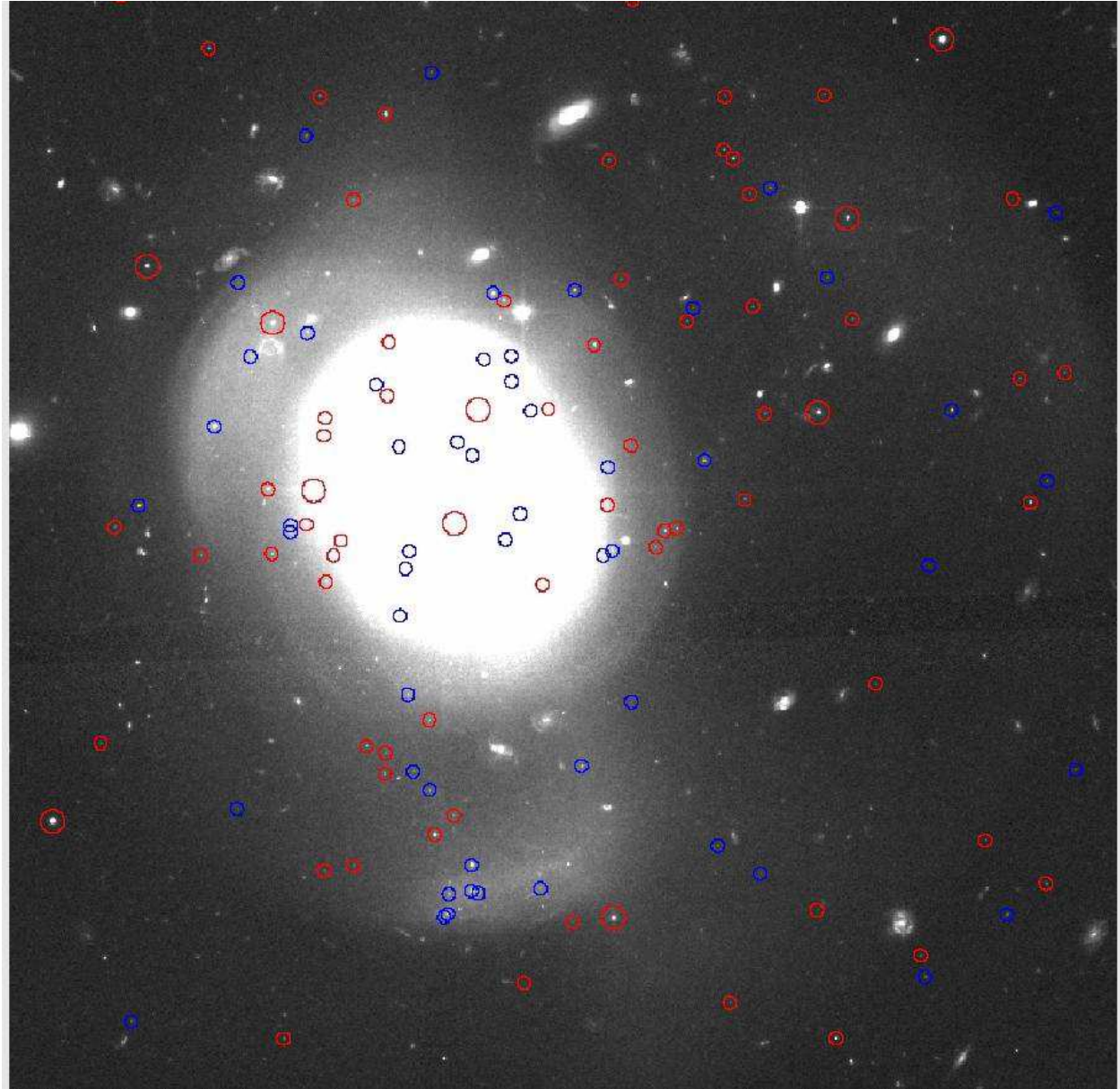


Fig. 9.— AM 0139-655 through the F814W filter. The frame is $84'' \times 84''$. The directions on the sky are same as in Fig. 1. The blue and the red circles represent the blue and the red clusters respectively. Clusters with I brighter than 24 mag are shown by the big red circles and clusters with I fainter than 24 mag are shown by the small red circles. Note that the bright shell to the East of the galaxy is populated exclusively by blue clusters.

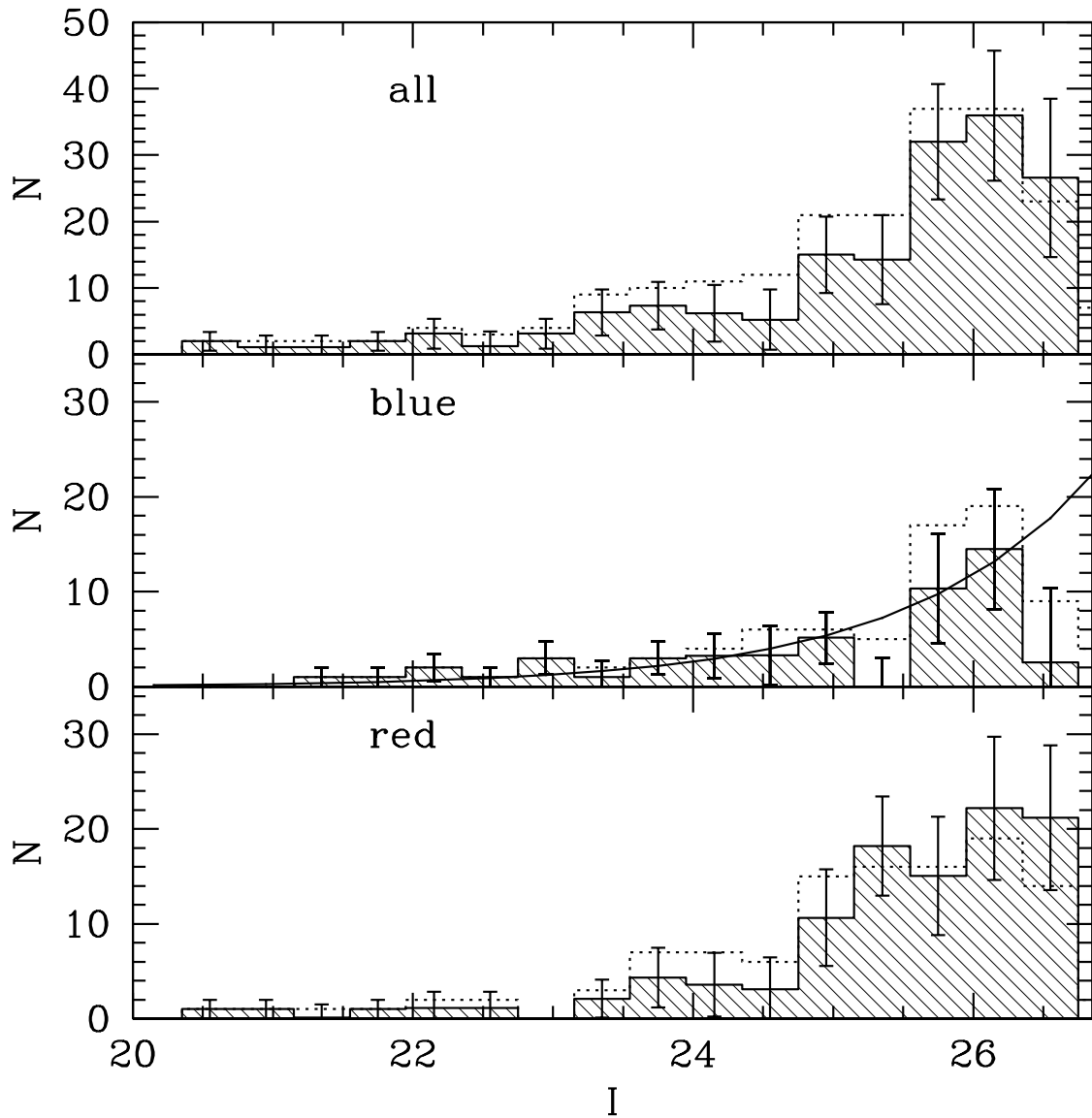


Fig. 10.— The luminosity function of clusters in AM 0139-655 in the I band. The dotted histograms mark uncorrected (observed) LFs and the hatched histograms mark LFs corrected for completeness and background contamination. Completeness-weighted error bars are also plotted. The top panel shows the combined luminosity function of all the clusters. The middle panel shows the luminosity function of the blue clusters and the power law fit, giving an index $\alpha \sim -1.8$. The lower panel shows the luminosity function of the red clusters.

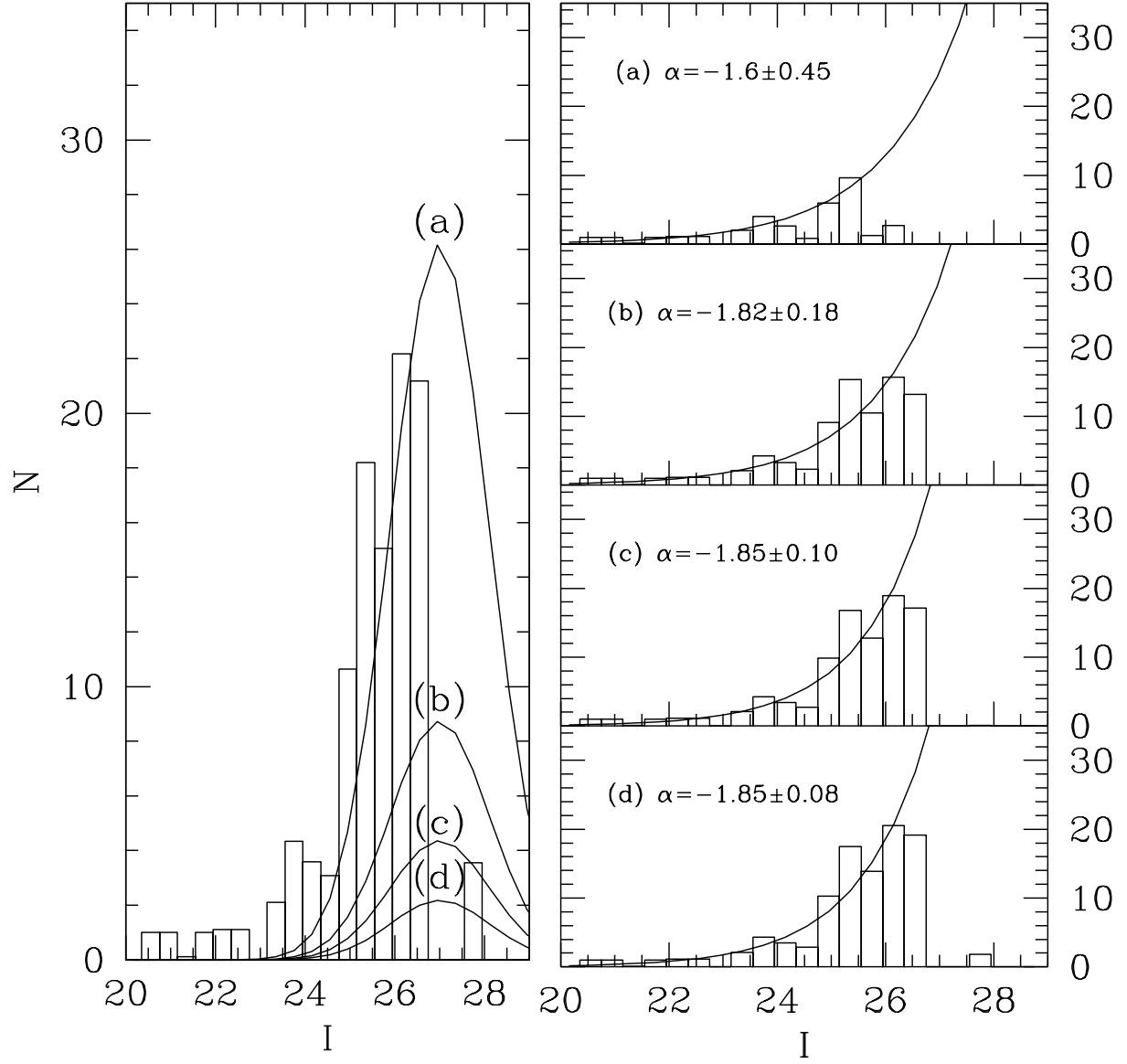


Fig. 11.— The left panel is the luminosity function (histogram) of the red clusters. The curves a,b,c and d stand for estimated Gaussians representing the old metal-poor GC population with specific frequencies of 3.0, 1.0, 0.5 and 0.25 respectively. The histograms in the right panel shows the luminosity functions of the clusters obtained after subtracting the contribution from each of the gaussians in the left panel. The solid lines in the right panels are power-law fits to the remaining clusters. Note that these clusters can be fit by a power-law (solid line) with $-1.6 \leq \alpha \leq -1.85$ as expected for young GCs. See Sect. 6.2 for a detailed discussion.

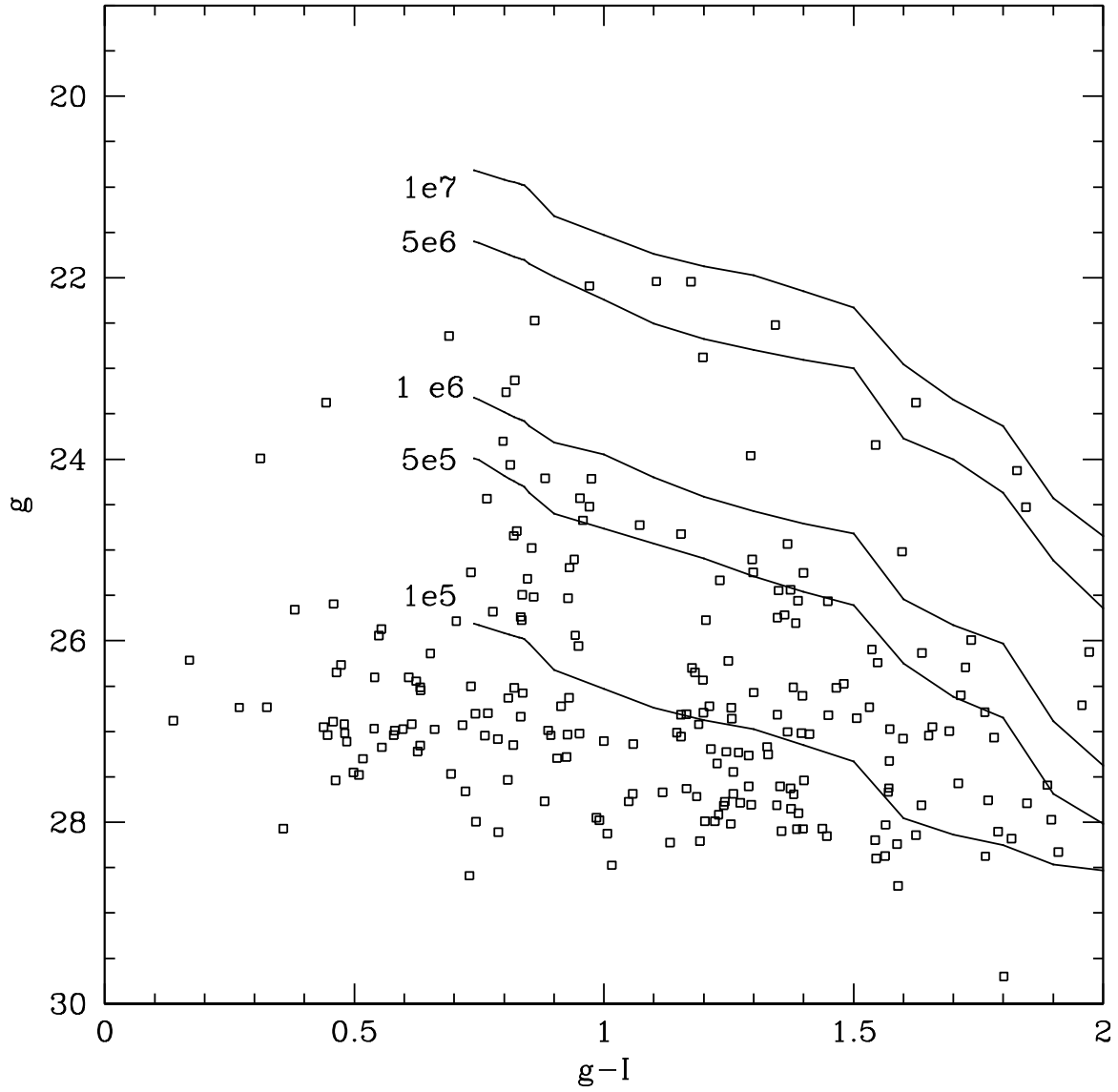


Fig. 12.— The CMD of the clusters associated with AM 0139-655. Superimposed are curves of constant mass (in units of M_{\odot}). All curves are computed for solar metallicity with ages ranging from 0.3 Gyr at the leftmost point to 14 Gyr at the right extreme for each curve. The masses are the masses of individual clusters after fading them to 14 Gyr and which have current color and magnitudes as specified in the plot. Note that AM 0139-655 harbors several very massive red clusters. It is clear that several of these clusters will end up with masses equal to or greater than that of ω Cen.